Water Research 188 (2021) 116465

Contents lists available at ScienceDirect

Water Research

journal homepage: www.elsevier.com/locate/watres

Dechlorination of 2,4-dichlorophenol in a hydrogen-based membrane palladium-film reactor: Performance, mechanisms, and model development

Chengyang Wu[a,b], Luman Zhou[a,b], Yun Zhou[c], Chen Zhou[d], Siqing Xia[a,b,*], Bruce E. Rittmann[d]

[a] State Key Laboratory of Pollution Control and Resource Reuse, College of Environmental Science and Engineering, Tongji University, Shanghai 200092, China
[b] Shanghai Institute of Pollution Control and Ecological Security, Shanghai 200092, China
[c] University of Alberta, Department of Civil and Environmental Engineering, Edmonton, AB, Abbreviation:
[d] Biodesign Swette Center for Environmental Biotechnology, Arizona State University, United States

ARTICLE INFO

Article history:
Received 28 July 2020
Revised 20 September 2020
Accepted 24 September 2020
Available online 28 September 2020

Keywords:
Hydrodechlorination
2,4-dichlorophenol
Membrane palladium-film reactor
Mathematical model

ABSTRACT

We created a hydrogen-based membrane palladium-film reactor (MPfR) by depositing palladium nanoparticles (PdNPs) on hollow-fiber membranes via autocatalytic hydrogenation to form a Pd-film. The MPfR was used for hydrodechlorination (HDC) of 2,4-dichlorophenol (2,4-DCP). HDC performances and mechanisms were systematically evaluated, and a continuous-flow dechlorination model was established. Approximately 87% of the input 2,4-DCP was reduced to the end-product phenol (P), while 2-chlorophenol (2-CP) was an intermediate, but only at 2%. Selective adsorption of the 2,4-DCP onto the Pd-film and fast desorption of P facilitated efficient dechlorination. Modeling results represented well the concentrations of 2,4-DCP and its intermediates. It demonstrated three dechlorination pathways: The majority of 2,4-DCP was completely dechlorinated to P in an adsorbed state without release of monochlorphenol, some 2,4-DCP was degraded to 2-CP that was released and subsequently adsorbed and reduced to P, and a small amount was reduced to 4-CP that was released and subsequently adsorbed and reduced to P. Analysis based on Density Functional Theory suggests that the pathway of full dechlorination was dominant due to its thermodynamically favorable adsorption configuration, with both Cl atoms bonded to Pd. This study documents full dechlorination of 2,4-DCP in the MPfR and the interacting roles of adsorption and HDC.

1. Introduction

Chlorophenols (CPs), which are widely used in the manufacture of herbicides, insecticides, wood preservative, dyes, and plant-growth regulators (Buchel 1984; Estevinho et al., 2007; Juhler et al., 2001; Li 2007), are toxic, carcinogenic, bioaccumulating, and slowly biodegradable (Vallecillo et al., 1999; Xu et al., 2013; Zhang et al., 2005). For instance, 2,4-dichlorophenol (2,4-DCP) is listed as a priority pollutant by the Ministry of Ecology and Environment of China (Yue et al., 2008) and the Environmental Protection Agency (EPA) of the United States (U.S. EPA. 2012), and its maximum contaminant level in drinking water is 0.1 $mg{\cdot}L^{-1}$. 2,4-DCP has been detected in surface waters (Gao et al., 2008) and contaminated soils (Witthuhn et al., 2005a; Witthuhn et al., 2005b), where it causes ecological human health risks (Vallecillo et al., 1999). Because its dechlorinated end-product (phenol) is relatively more biodegradable and less toxic, dechlorination of 2,4-DCP is a promising method for 2,4-DCP treatment.

Using hydrogen gas (H_2) as the electron donor, catalytic hydrodechlorination (HDC, also known as reductive dechlorination) on palladium (Pd) nanoparticles (PdNPs) has emerged as a sustainable alternative that facilitates fast kinetics, high efficiency, operation under mild conditions, and no secondary waste stream (Diaz et al., 2016; Yuan and Keane 2003b). Highly reductive atomic hydrogen is generated on the Pd surface by homolytic cleavage of adsorbed H_2, which is activated to substitute the Cl atoms in CPs (Chaplin et al., 2012; Conrad et al., 1974; Fu et al., 2019). However, the safe and efficient H_2 delivery in practical application is challenging (Chaplin et al., 2012). In additional, PdNPs normally need to be dispersed and stabilized on suitable supporting materials to acquire high-active and long-term sustainability (Benitez and Del Angel 2000; Deng et al., 2014; Yuan and Keane 2003a).

* Corresponding author.
E-mail address: siqingxia@gmail.com (S. Xia).

https://doi.org/10.1016/j.watres.2020.116465
0043-1354/

The H_2-based membrane palladium-film reactor (MPfR) efficiently delivers H_2 to PdNPs by permeation through the walls of hollow-fiber membranes in a bubble-free way (Zhou et al., 2016). The maximum H_2-delivery capacity is determined by the H_2 permeability in the membranes material and can be controlled by regulating the H_2 pressure (Tang et al., 2012). The membranes can be the support and stabilizer for the PdNPs (Zhou et al., 2016) that are generated *in situ* via an autocatalytic reduction of Pd(II) to metallic palladium (Pd(0)) to form PdNPs (Besson et al., 2005). This autocatalytic deposition of PdNPs executed in the MPfR avoids risks of H_2 bubbling and complications associated with conventional supporting materials, like activated carbon (Diaz et al., 2016; Soares et al., 2009), metallic oxide (Gao et al., 2017; Kim et al., 2013), multiwall carbon nanotubes (Deng et al., 2014; Xu et al., 2016b; Xu et al., 2012; Zhao et al., 2016).

Previous studies on the kinetics of catalytic HDC were executed in sequencing batch experiments (Wang et al., 2013; Xu et al., 2016a; Xu et al., 2016b; Zhao et al., 2016). Existing kinetic models cannot simulate entire HDC process in continuous flow reactors that are used in practical application. Since stepwise HDC that leads to accumulation of lower CPs in the liquid presents a risk for water pollution due to the higher solubilities of the less-chlorinated phenols (Cho et al., 2000), it would be meaningful to develop a mathematical model that describes the fate of 2,4-DCP and its dechlorinated products for continuous flow. CPs transformation pathways can be deduced from the reduction kinetics.

The over-arching objective of this study was to systematically evaluate HDC of 2,4-DCP using a MPfR operated in continuous mode. Specific objectives were (1) to analyze the content and structural characteristics of the deposited PdNPs; (2) to explore adsorption behaviors of 2,4-DCP, 2-chlorophenol (2-CP), 4-chlorophenol (4-CP), and phenol (P) on the Pd-film; (3) to assess the kinetics and mechanism of HDC of 2,4-DCP; and (4) to develop and apply an HDC model that can simulate the effluent concentrations of 2,4-DCP and its dechlorinated products. The adsorption-reduction process on Pd(0) surface was interpreted using Density Functional Theory (DFT) to reveal the relationship between adsorption and HDC in the MPfR.

2. Materials and methods

2.1. Chemicals and materials

Disodium tetrachloropalladate (Na_2PdCl_4, 98.0%), 2,4-dichlorophenol (99.5%), 2-chlorophenol (99.0%), 4-chlorophenol (99.0%), and phenol (99.5%) were purchased from Aldrich (USA). Disodium hydrogen phosphate (Na_2HPO_4, 99.0%) and potassium dihydrogen phosphate (KH_2PO_4, 99.5%) were obtained from Sinopharm Group (China). Hydrogen gas (H_2, 99.99%), and nitrogen gas (N_2, 99.99%) was supplied by Chunyu Special Gas (China). 5-mM phenols stock solutions were prepared by dissolving them in deoxygenated water and stored at 4 °C, which were added into influent water during adsorption and dechlorination experiments. To stable pH, 2-mM phosphate buffer (Na_2HPO_4 + KH_2PO_4) was added to the influent across the whole experiments.

2.2. Experimental setup

A schematic of the MPfR used in this study is in Figure S1, Supporting Information (SI). The MPfR included two glass tubes connected by polytetrafluoroethylene (PTFE) tubing (Norprene Chemical, Saint-Gobain, USA), had a 70-mL working volume, and contained two bundles of nonporous polypropylene hollow-fiber membranes (200-μm outer diameter, 100–110-μm inner diameter, Teijin, Japan) with a total membrane surface area of 54 cm^2. The main column contained 32 hollow-fiber membranes, while the other column contained 10 fibers used as Pd-film sampling coupons. The fibers of the main bundles were glued at both ends and connected to a H_2 gas supply, while the coupon bundles had only an upper H_2 gas supply. H_2 gas was constantly supplied to fiber bundles at 2 atm (absolute pressure) adjusted by a pressure regulator, and it diffused through the fiber walls in a bubble-free manner. The maximum H_2-delivery capacity (0.37 g $H_2 \cdot m^{-2} \cdot day^{-1}$), calculated according to Tang et al. (2012), was sufficient for Pd reduction to form PdNPs and for complete HDC of 2,4-DCP in all experiments. The liquid contents of the MPfR was well mixed through a recirculation rate of 100 $mL \cdot min^{-1}$ achieved by a peristaltic pump (model 1515X, Longer, China). Thus, the solute concentrations inside the MPfR were equal to its effluent concentrations. The temperature was maintained at 25 ± 1°C.

2.3. Preparation and characterization of PdNPs-film

For deposition of PdNPs on the surface of the hollow-fiber membranes, medium contained Pd(II) (1 mM as Na_2PdCl_4) and 2-mM phosphate buffer (pH = 7.2) was purged with N_2 gas to eliminate dissolved oxygen (DO < 0.15 $mg \cdot L^{-1}$). The medium was then pumped into the MPfR, which was run in batch mode for 2 days to produce a film of PdNPs on the fibers. Pd(II) concentrations in solution were analyzed by inductively coupled plasma optical emission spectrometer (ICP-OES; Agilent 720ES, USA) at a wavelength of 340.46 nm. The coating process was repeated three times until that a thick PdNPs-film accumulated on the fibers and at least 99% of the input soluble Pd(II) was reduced by H_2 in each time.

To examine the PdNPs, we recorded a Powder X-ray diffraction (XRD) pattern using an X' Pert PRO MPD diffractometer with Cu-Kα (wavelength 1.54 Å, 40 kV, 55 mA) radiation and 0.5° grazing incidence angle. An X-ray photoelectron spectrum (XPS; Thermo ESCALAB 250, USA) was used to characterize the Pd oxidation state of the Pd-film. A scanning electron microscopy (SEM; Zeiss Sigma 300, German) and a transmission electron microscopy (TEM; JEOL JEM 2100F, Japan) equipped with an energy dispersive X-ray detector (EDX) were used to obtain the morphology characteristics of PdNPs immobilized on the fibers.

2.4. Adsorption experiments

Equilibrium adsorption experiments was performed after a Pd-film formed on the fiber surface. The MPfR was set to a batch mode to explore the adsorption of 2,4-DCP, 2-CP, 4-CP, or P onto the Pd-film. The H_2 supply was disconnected, and the liquid medium was replaced by 70 mL of new medium contained 2,4-DCP at desired concentrations (25, 55, 100, or 200 μM), and then 2,4-DCP was replaced by 2-CP, 4-CP, or P successively at the same concentrations. Between each experiment, the MPfR was rinsed with alcohol and distilled water to remove adsorbed phenols until the solute became undetectable in the rinse water. When solute concentrations had reached equilibrium, we measured the concentration of the solute in liquid and computed the mass of adsorbed phenols by difference.

The adsorption capacities of Pd-film for the phenols could be represented well using the Langmuir isotherm:

$$Q_e = \frac{Q_0 C_t}{C_t + b^{-1}} \quad (1)$$

where Q_e ($mmol \cdot g_{cat}^{-1}$) is the equilibrium adsorption density, Q_0 ($mmol \cdot g_{cat}^{-1}$) and b^{-1} ($mmol \cdot L^{-1}$) are Langmuir constants for the maximum adsorption capacity and the affinity concentration, respectively, and C_t is the equilibrium solute concentration ($mmol \cdot L^{-1}$).

The adsorption kinetics of 2,4-DCP, 2-CP, 4-CP, or P were evaluated in batch experiments with an initial concentration of 200 μM.

The loss of the solute was represented well by a pseudo-second-order rate, which can be described by its linear form as:

$$\frac{t}{q_t} = \frac{1}{K_2 q_e^2} + \frac{t}{q_e} = \frac{1}{v_0} + \frac{t}{q_e} \quad (2)$$

where K_2 ($g_{cat}{\cdot}mmol^{-1}{\cdot}min^{-1}$) is the rate constants of pseudo second-order adsorption; v_0 was the initial adsorption rate ($mmol{\cdot}min^{-1}{\cdot}g_{cat}{}^{-1}$); and q_e and q_t are amount of the phenols adsorbed onto the Pd-film ($mmol{\cdot}g_{cat}{}^{-1}$) at equilibrium and at time t (min), respectively.

2.5. Dechlorination experiments

Experiments for HDC of 2,4-DCP, 2-CP, and 4-CP were executed after completion of the adsorption experiments. Before each experiment, the MPfR was purged and refilled with influent medium, the H_2 supply was turned on, and the MPfR was shifted to continuous mode with an influent flow rate of 0.265 $mL{\cdot}min^{-1}$. The influent concentrations of 2,4-DCP, 2-CP, or 4-CP were set at 25, 55, 100, or 200 μM, respectively, for the different experiments.

2.6. Sampling and analyses

We collected liquid samples from the MPfR at preselected time intervals and immediately filtered them through PTFE syringe filters (0.22 μm). The concentrations of 2,4-DCP, 2-CP, 4-CP, and P were measured by gas chromatography-mass spectrometer (GC–MS, Trace DSQ, USA) equipped with a DB-5MS column (30 m × 0.25 mm × 0.25 μm film thickness) and high-performance liquid chromatography (HPLC, Shimadzu Prominence LC-20A, Japan) equipped with an Agilent C18 column (250 × 4.6 mm) and a diode-array detector. The mobile phase was a mixture of acetonitrile and ultrapure water (with 0.1% acetic acid) in the volume proportion of 65:35. The flow rate of HPLC pump was controlled at 1.0 $mL{\cdot}min^{-1}$, and the UV detector was set at 190 nm. We also collected unfiltered samples to analyze the Pd concentration in effluent and digested them by thickish hot mixture of nitric acid and hydrochloric acid before analyzing, and no Pd(II) was detected in liquid samples from adsorption and dechlorination experiments.

2.7. Mathematical model for HDC

We represented the MPfR as continuous stirred tank reactor (CSTR) with an immobilized catalyst. The mass balance on a solute is:

$$V\frac{dC_i}{dt} = QC_0 - QC_e + Vr \quad (3)$$

in which

$$r = -kC_i \quad (4)$$

where C_0, C_i, and C_e (μM) are solute concentrations in the influent, the bulk in reactor, and the effluent, respectively; Q ($mL{\cdot}min^{-1}$) is influent flow rate of the reactor; t is time (min); V is the working volume of reactor (70 mL); and k is a first-order reaction rate constant for the solute (min^{-1}) (Wang et al., 2013; Xu et al., 2016b; Zhao et al., 2016).

Because the liquid in the reactor was uniformly mixed, the solute concentration inside a MPfR was equal to its effluent concentration ($C_i = C_e$). Substitution of Eq. (4) into Eq. (3) and rearrangement yields

$$\frac{dC_e}{dt} - \frac{Q}{V}C_0 + \frac{Q}{V}C_e = -kC_e \quad (5)$$

2,4-DCP can be reductively dechlorinated in via three pathways (shown in Fig. 1), in which H· is an active-hydrogen atom and e^- is an electron:

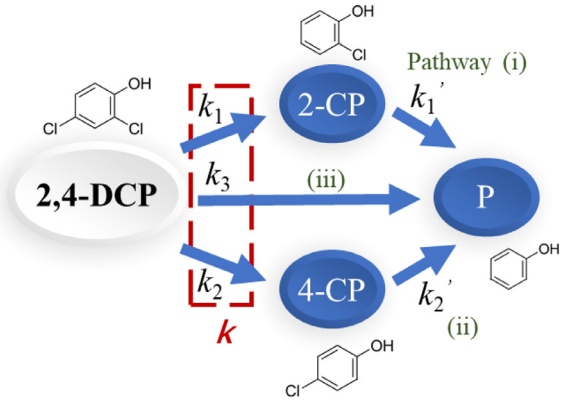

Fig. 1. Schematic of the HDC pathways for 2,4-DCP.

$$2,4-DCP + H\cdot + e^- \xrightarrow{k_1} 2-CP + Cl^- \quad (6)$$

$$2-CP + H\cdot + e^- \xrightarrow{k_1'} P + Cl^- \quad (7)$$

$$2,4-DCP + H\cdot + e^- \xrightarrow{k_2} 4-CP + Cl^- \quad (8)$$

$$4-CP + H\cdot + e^- \xrightarrow{k_2'} P + Cl^- \quad (9)$$

$$2,4-DCP + 2H\cdot + 2e^- \xrightarrow{k_3} P + 2Cl^- \quad (10)$$

Reaction (10) is a two-electron reductive dechlorination in which the product of the first dechlorination step (2-CP or 4-CP) remains adsorbed and rapidly undergoes the second dechlorination step; thus, neither 2-CP nor 4-CP appears as an intermediate of reaction (10).

Because previous studies have shown that the dechlorination reactions of CPs by PdNPs follow pseudo-first-order kinetics (Wang et al., 2013; Xu et al., 2016b; Zhao et al., 2016), the corresponding rate expressions for the disappearance of 2,4-DCP, the transient formation of intermediates (2-CP and 4-CP), and the accumulation of end-product P in the CSTR are:

$$\frac{dC_{e(2,4-DCP)}}{dt} - \frac{Q}{V}C_{0(2,4-DCP)} + \frac{Q}{V}C_{e(2,4-DCP)} = -kC_{e(2,4-DCP)} \quad (11)$$

$$\frac{dC_{e(2-CP)}}{dt} + \frac{Q}{V}C_{e(2-CP)} = k_1C_{e(2,4-DCP)} - k_1'C_{e(2-CP)} \quad (12)$$

$$\frac{dC_{e(4-CP)}}{dt} + \frac{Q}{V}C_{e(4-CP)} = k_2C_{e(2,4-DCP)} - k_2'C_{e(4-CP)} \quad (13)$$

$$\frac{dC_{e(P)}}{dt} + \frac{Q}{V}C_{e(P)} = k_1'C_{e(2-CP)} + k_2'C_{e(4-CP)} + k_3C_{e(2,4-DCP)} \quad (14)$$

in which

$$k = k_1 + k_2 + k_3 \quad (15)$$

The effluent concentration of 2,4-DCP, 2-CP, 4-CP, and P can be obtained by integrating Eqs. (11) - (14):

$$C_{e(2,4-DCP)} = \frac{C_{0(2,4-DCP)}}{Q+kV}\left(Q + kVe^{-\frac{Q+kV}{V}\cdot t}\right) \quad (16)$$

$$C_{e(2-CP)} = \frac{k_1V\cdot C_{0(2,4-DCP)}}{k_1' - k}\left(\frac{k}{Q+kV}e^{-\frac{Q+kV}{V}\cdot t} - \frac{k_1'}{Q+k_1'V}e^{-\frac{Q+k_1'V}{V}\cdot t}\right) + \frac{k_1QV\cdot C_{0(2,4-DCP)}}{(Q+kV)(Q+k_1'V)} \quad (17)$$

$$C_{e(4-CP)} = \frac{k_2 V \cdot C_{0(2,4-DCP)}}{k_2' - k}\left(\frac{k}{Q+kV}e^{-\frac{Q+kV}{V}\cdot t} - \frac{k_2'}{Q+k_2'V}e^{-\frac{Q+k_2'V}{V}\cdot t}\right) + \frac{k_2 QV \cdot C_{0(2,4-DCP)}}{(Q+kV)(Q+k_2'V)} \quad (18)$$

$$C_{e(P)} = C_{0(2,4-DCP)} - C_{e(2,4-DCP)} - C_{e(2-CP)} - C_{e(4-CP)} \quad (19)$$

In a similar way, when the continuous influent in the MPfR is 2-CP or 4-CP, the effluent concentration is

$$C_{e(2-CP)} = \frac{C_{0(2-CP)}}{Q+k_1'V}\left(Q + k_1' V e^{-\frac{Q+k_1'V}{V}\cdot t}\right) \quad (20)$$

$$C_{e(4-CP)} = \frac{C_{0(4-CP)}}{Q+k_2'V}\left(Q + k_2' V e^{-\frac{Q+k_2'V}{V}\cdot t}\right) \quad (21)$$

In order to obtain the data for model fitting, we conducted three series experiments (shown in Figure S2, SI), in which 2,4-DCP, 2-CP and 4-CP were added, respectively. And the detail solving process is provided in Supporting Information.

3. Results and discussion

3.1. Characterization of the Pd-film

Over 6 days in the batch mode, over 99% of the Pd(II) was reduced to Pd(0) that nucleated on the MPfR's membrane surface and formed a black film having an average Pd density of 7.5 g Pd·m^{-2} membrane (a total of 40 mg Pd). The XRD spectra of freeze-dried sample collected from the fibers (Figure S3a in SI) exhibited the four Pd(0) peaks: 40.1° (1 1 1), 46.7° (2 0 0), 68.1° (2 2 0), and 82.1° (3 1 1) (JCPDS No.46–1043). Pd(0) was further confirmed by XPS analysis (Figure S3b in SI), with the peaks at 340.7 and 335.5 eV corresponding to the typical $3d_{3/2}$ and $3d_{5/2}$, respectively (Zhou et al., 2017). The XPS spectra also reveals tiny fractions of unreduced Na_2PdCl_4 (4.3%) and PdO (9.7%) on PdNPs surfaces. Because the MPfR was oxygen-free (DO < 0.15 mg/L), the PdO was likely created from surface oxidation during sample preparation procedure, such as mashing of the Pd solid. Moreover, characteristic peaks of PdO did not appear in the XRD spectra, which indicates negligible amounts of PdO retained. These results document that Pd(0) formed on the fiber surface.

SEM and TEM images characterize the morphology of the Pd-film. Fig. 2a shows the surface of the Pd-film was rough and compact. A closer look (Fig. 2b) reveals the massive accumulated PdNPs and pores on this rough surface, and indicates that the Pd(0) crystallites formed into larger particles. The results manifest that the Pd-film is the aggregation of PdNPs and possesses the porous structure. TEM-EDX elemental mapping (Figure S3c) of a cross section of Pd-film provides further evidence of stabilization of PdNPs. Fig. 2c shows a multi-layer dark black film stably attached to the fiber surface. Individual Pd(0) crystallites, with an average size of 12.4 ± 0.9 nm (110 counts), can be observed on a PdNPs layer (Fig. 2d), and their characteristic lattice fringes dominated by the (1 1 1) D-spacing of 2.3 Å (Khan et al., 2014). Calculations in SI indicate that this level of PdNP coverage corresponded to approximately 66 layers of 12.4-nm crystallites packed on the membrane surface. The theoretical maximum specific surface area of the Pd-film was 40 $m^2 \cdot g_{cat}^{-1}$, and the calculated film thickness was 670 nm, a value close to the average thickness of ~710 nm obtained from image areas in Fig. 2c and Figure S3c, which infers the accumulated structure of the PdNPs is approximate to be hexagonal close packed structure.

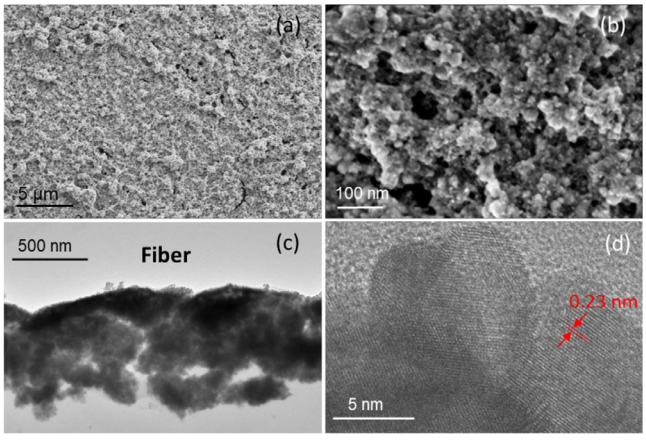

Fig. 2. SEM and TEM images of a single fiber with Pd-film fixed and collected at the end of batch mode. (a) SEM images of the Pd-film surface (10 000 ×). (b) A chosen area that shows the morphology of PdNPs accumulated on the surface (270 000 ×). (c) Boundary of the fiber and the Pd-film (25 000 ×). (d) The lattice fringes of the Pd(0) crystallites (1500 000 ×).

3.2. Adsorption kinetics and isotherms of 2,4-DCP by Pd-film

Results of adsorption experiments (shown in Figure S4, SI) show that the four phenolic compounds had fast initial adsorption to the Pd-film, and adsorption equilibrium was achieved within 5 min for all experiments. The highest adsorption capacity was for 2,4-DCP (up to 0.092 mmol·g_{cat}^{-1}), followed by 4-CP (0.066 mmol·g_{cat}^{-1}), 2-CP (0.060 mmol·g_{cat}^{-1}), and P (0.015 mmol·g_{cat}^{-1}).

The pseudo-second-order adsorption kinetics of 2,4-DCP, 2-CP, 4-CP, and P by the Pd-film are summarized in Table 1. The v_0 followed the order of 2,4-DCP > 4-CP ≥ 2-CP >> P. More electronegative chloro substituents led to increased affinity (q_e) to the Pd surface, and this correlated to a larger v_0 value, since the K_2 kinetic coefficients were 5 ~ 6 g_{cat}·mmol^{-1}·min^{-1}, for 2,4-DCP, 2-CP, and 4-CP. Phenol's K_2 value was much larger, which supports that its transport away from the Pd-film was not rate limiting.

The Langmuir isotherm using the Q_0 and $1/b$ values in Table 1 could represent well equilibrium adoption of all solutes: r^2 value ≥ 0.99 and no systematic errors (Figure S5). Q_0, the indicator of adsorption capacity, was in the order 2,4-DCP > 4-CP ≥ 2-CP >> P, almost the same relationship for q_e from the kinetic experiments and consistent with computations from DFT for the adsorption energy of 2,4-DCP on PdNPs supported on carbon or titanium nitride (Fu et al., 2019; Yuzhuo Chen 2019). The $1/b$ affinity concentrations declined in the same order as Q_0, which indicates that solutes with higher adsorption capacity required a higher solute concentration to approach their capacity.

The Langmuir isotherm represents monolayer adsorption on distinct localized adsorption sites, with no adsorbate mobility among the sites (Langmuir 1918). It also requires negligible interactions, such as steric hindrance, between the adsorbed phenols. The estimated 2,4-DCP coverage ratio on the PdNPs surface (q_r) was 0.54 (calculations are in SI), which supports that adsorption was not more than a monolayer coverage.

3.3. Reductive dechlorination of 2,4-DCP in the MPfR

In the reductive dechlorination experiments, the influent concentrations of 2,4-DCP were 25, 55, 95, or 195 μM. Fig. 3 presents the effluent concentrations of 2,4-DCP and its dechlorinated products (2-CP, 4-CP, and P) over 6 h of continuous operation; Table S1 summarizes the average concentrations in the effluent and their coefficients of variation during the period from 2 h to 6 h. Rapid adsorption of 2,4-DCP caused the gap of mass balance (closure of 90.1 ± 3.0%) in the first 5 min of the experiments. Then, 2,4-DCP approached steady-state removal of approximately 92%.

Table 1
Parameters for the adsorption kinetics and isotherms of 2,4-DCP, 2-CP, 4-CP, and P by the Pd-film at 298 K.

Model	Parameter	2,4-DCP	2-CP	4-CP	P
Pseudo-second-order (C_0 = 200 μM)	q_e, mmol·g_{cat}^{-1}	0.175	0.140	0.137	0.026
	K_2, g_{cat}·$mmol^{-1}$·min^{-1}	5.08	5.83	5.97	31.1
	v_0, mmol·min^{-1}·g_{cat}^{-1}	0.043	0.021	0.026	0.007
	r^2	0.993	0.996	0.988	0.972
Langmuir	Q_0, mmol·g_{cat}^{-1}	0.148	0.094	0.097	0.015
	b^{-1}, mmol·L^{-1}	0.149	0.103	0.079	0.015
	r^2	0.992	0.991	0.997	0.989

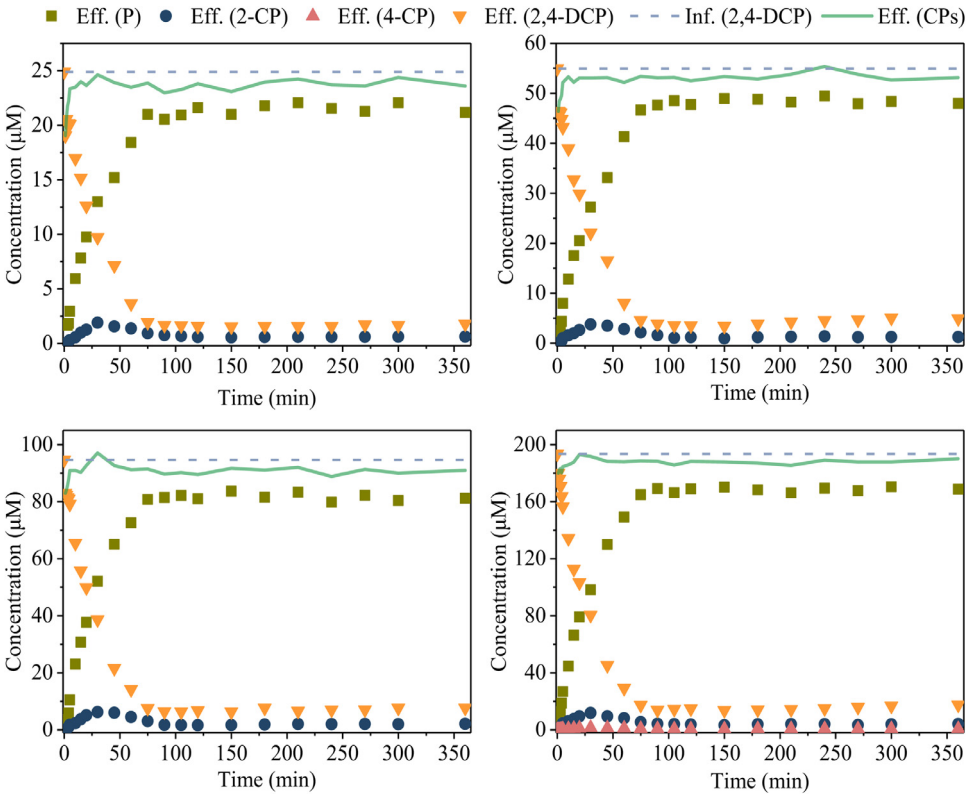

Fig. 3. The effluent concentrations of 2,4-DCP, 2-CP, 4-CP, and P over time at different influent concentration of 2,4-DCP, during initial 6 h. Notes: The line represents the sum of CPs, and 4-CP was undetected except for (d).

The monochlorphenols (MCPs, *i.e.* 2-CP and 4-CP) had small peaks around 30 min, but then decreased to a steady, low value, about 2% of influent 2,4-DCP. The concentration of P increased to a stable concentration that was about 87% of the influent concentration of 2,4-DCP. Over the last 4 h, the measured concentrations accounted for 96.5 ± 0.8% of the input 2,4-DCP. GC–MS results showed no other products besides 2-CP, 4-CP, and P during the dechlorination process. This small deficiency in the mass balance probably can be attributed to volatilization during sampling and analysis, because volatilization tests showed an average 6% loss of 2,4-DCP during experimental operation without Pd loading or H_2 supplying (Figure S6, SI).

2-CP was detected in all series, but 4-CP was only detected at $C_{0(2,4\text{-DCP})}$ = 200 μM. This supports that the reactivity of C–Cl at *para*-position is higher than that of C–Cl at *ortho*-position, possibly due to steric hindrance at *ortho*-position than that at *para*-position (Sun et al., 2014).

3.4. Kinetics and mechanisms for 2,4-DCP dechlorination

As revealed in Figs. 4 and 5, stable effluent patterns were achieved within 2 h for all CPs species and concentrations. For 2,4-DCP reduction experiments, the measured concentrations of intermediate MCPs during the initial 2 h were slightly lower than that fitted by the model (dotted line in Fig. 4). Simultaneously, the average mass balance closure during initial 2 h (94.3%) was lower than that in the steady state (96.5%). This discrepancy reflects some phenols were adsorbed on the Pd-film. However, it was unlikely due to the adsorption of 2,4-DCP or P as the adsorption equilibrium was achieved within 5 min for 2,4-DCP, and P featured low adsorption capacity and fast transport rate (discussed in Section 3.2). Therefore, the adsorption of MCPs causes the experiment data of MCPs concentrations are lower than the model results.

Based on the identified dechlorinated products, the transformations of 2,4-DCP in MPfR followed the steps shown in Eqs. (6) - (10). Substitution of the measured effluent concentrations after 5 min into Eqs. (15) - (21) led to the HDC-rate constants k, k_1, k_2, k_3, k_1', and k_2' displayed in Table 2. These parameters gave good fits with relatively high correlation coefficients (all $r^2 \geq 0.98$) and without systematic errors. Assuming that the overall kinetics were controlled by the catalytic reaction is supported by the initial adsorption rate of 2,4-DCP (v_0 = 0.043 mmol·min^{-1}·g_{cat}^{-1}, C_0 = 200 μM) being greater than the initial reduction rate (v_r = 0.013 mmol·min^{-1}·g_{cat}^{-1}, C_0 = 200 μM).

Table 2
Pseudo-first-order reduction rate constants for HDC of 2,4-DCP in the MPfR.

C_0/μM	k/min^{-1}	r^2	k_1/min^{-1}	r^2	k_2/min^{-1} [a]	r^2	k_1'/min^{-1}	r^2	k_2'/min^{-1}	r^2	k_3/min^{-1}	v_r [b]
25	0.0388	0.986	0.0112	0.995	\	\	0.0376	0.975	0.0345	0.980	0.0276	0.0017
55	0.0379	0.985	0.0103	0.983	\	\	0.0375	0.983	0.0338	0.983	0.0276	0.0036
95	0.0382	0.986	0.0096	0.987	\	\	0.0377	0.993	0.0345	0.989	0.0286	0.0064
195	0.0378	0.988	0.0090	0.979	0.0015	0.985	0.0373	0.983	0.0344	0.986	0.0288	0.0129

Notes: a. 4-CP was only detected with C_0 = 200 μM, and no k_2 values are possible for other concentrations; b. v_r is the reduction rate of 2,4-DCP (mmol·min^{-1}·g_{cat}^{-1}); $v_r = k \cdot C_i \cdot V / M_{cat}$, where M_{cat} is the mass of Pd in the MPfR (40 mg).

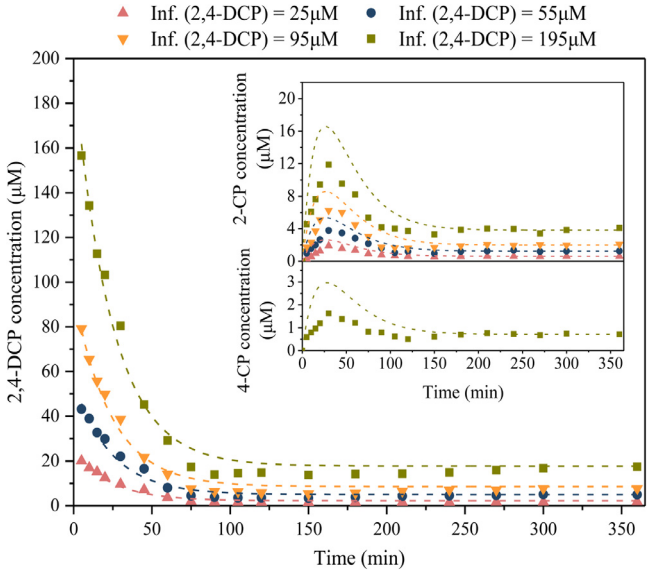

Fig. 4. Comparison of measured and calculated effluent concentrations in 2,4-DCP dechlorination experiments after 5 min (the dotted line is the model result and the scatter point are the experimental result).

The rate order was $k_3 >> k_1 >> k_2$, which indicates that successive dechlorinations without desorption of an MCP was the dominant pathway. Nearly 70% of 2,4-DCP was dechlorinated to P this way, followed by stepwise dechlorination via 2-CP at 26% and 4-CP at 4%. Because the dominant reaction did not require desorption of 2-CP or 4-CP, their accumulations of MCPs were small after 5 min.

The sequence of reductive-dehalogenation reactions of halogenated aromatic compounds generally follows the electron affinity of the electron acceptors present in anaerobic environments (Dolfing and Harrison 1992). We calculated the Gibbs free-energy change ($\triangle G^0$) of full and semi-dechlorination reactions:

$$2,4-\mathrm{DCP} + 2\mathrm{H_2} \rightarrow \mathrm{P} + 2\mathrm{Cl^-} + 2\mathrm{H^+},\ \Delta G^0 = -57.7\ \mathrm{kJ}\cdot\left(\mathrm{mole^-}\right)^{-1};$$

$$2,4-\mathrm{DCP} + \mathrm{H_2} \rightarrow 2-\mathrm{CP} + \mathrm{Cl^-} + \mathrm{H^+},\ \Delta G^0 = -52.9\ \mathrm{kJ}\cdot\left(\mathrm{mole^-}\right)^{-1};$$

$$2,4-\mathrm{DCP} + \mathrm{H_2} \rightarrow 4-\mathrm{CP} + \mathrm{Cl^-} + \mathrm{H^+},\ \Delta G^0 = -51.0\ \mathrm{kJ}\cdot\left(\mathrm{mole^-}\right)^{-1}.$$

Comparing the $\triangle G^0$ values, full dechlorination is thermodynamically favorable, and it is kinetically possible when the catalyst brings together two activated H·s with adsorbed 2,4-DCP and it still-adsorbed MCPs. Dechlorination of the *para*-Cl proceeded at a greater rate than *ortho*-Cl removal ($k_1/k_2 >> 1$), and this is consistent with published studies that ascribed this trend to steric constraints imposed by the *ortho*-Cl substituent (Shin and Keane 1999; Wei et al., 2006). Table 2 also shows that HDC of MCP intermediates was faster than for 2,4-DCP (*i.e.*, $k_1' \approx k_2' > k_1$ or k_2), which is consistent with an electrophilic aromatic substitution where the second electron-withdrawing Cl has a inactivating effect (Shin et al., 1999). It also explains why effluent concentrations of 2-CP and 4-CP were low.

Because adsorption precedes reduction, dechlorination of 2,4-DCP occurred in two steps: (1) 2,4-DCP adsorption to PdNP, with activation of the C–Cl bond; and (2) C–Cl bond breaking coupled electron-transfer from activated H· that also was adsorbed to the PdNPs. Jiang et al. (2018) calculated the adsorption energy (ΔE_{ads}) for typical adsorption configurations of 2,4-DCP's Cl atoms to Pd (1 1 1) plane (Table S2, SI). The adsorption configurations are illustrated in Fig. 6, they found that adsorption configuration (iii) with two Cl atoms bonded to Pd(0) is favorable based on its largest ΔE_{ads}, compared with single *para* (i) or *ortho* (ii) Cl bonds with Pd

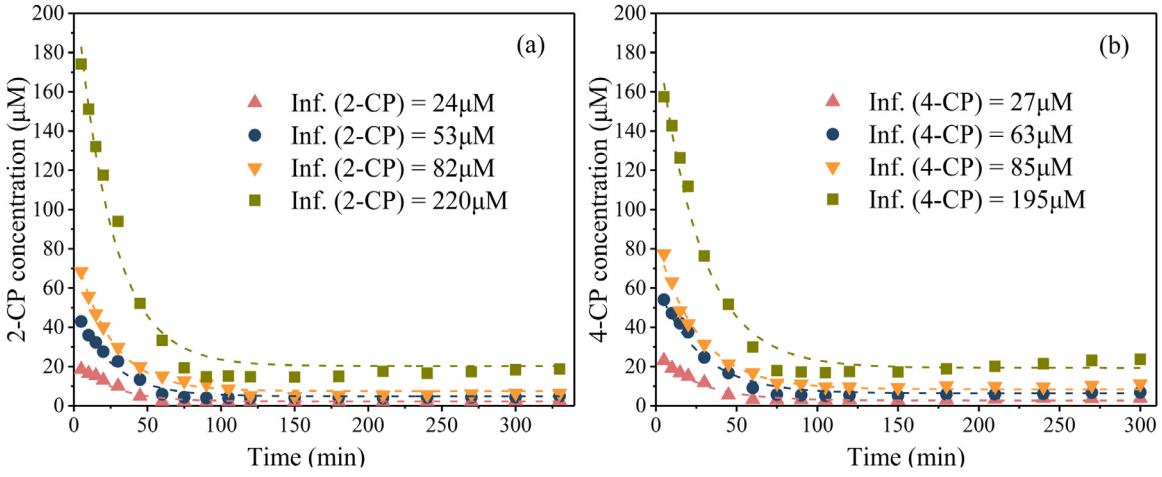

Fig. 5. Comparison of measured and calculated effluent concentrations in 2-CP (a) and 4-CP (b) dechlorination experiments after 5 min (the dotted line is the model result and the scatter point are the experimental result). The concentrations of P are shown in Figure S7 and S8, SI.

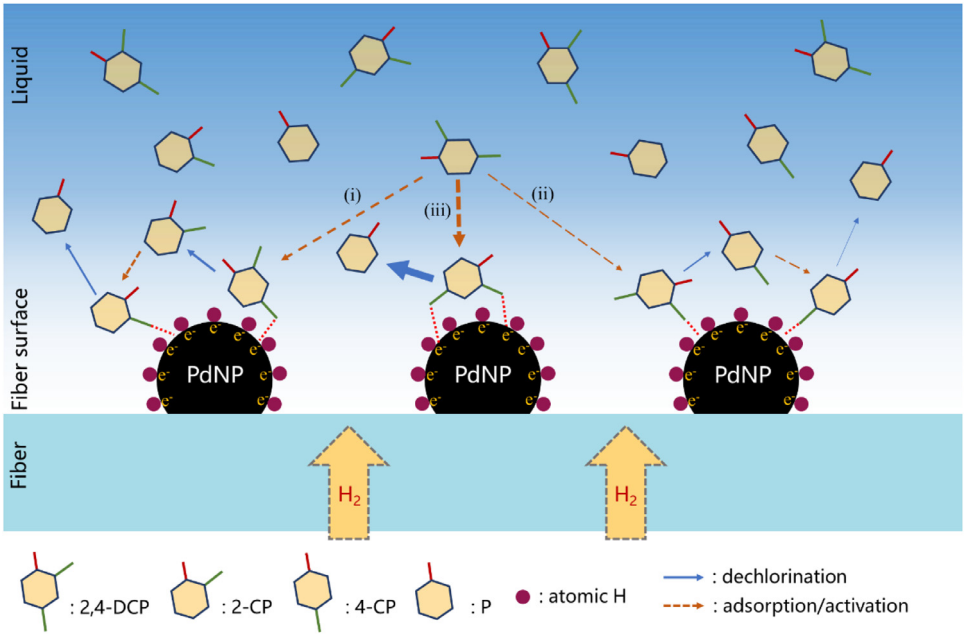

Fig. 6. Hypothetical mechanism of the adsorption-dechlorination pathways derived from DFT analysis (Jiang et al., 2018). Configuration (i) or (ii) is with single *para* or *ortho* Cl atom bonded with Pd atoms; configuration (iii) is with both the two Cl atoms bonded with Pd atoms.

atoms. This result supports that our findings that 2,4-DCP had the strongest adsorption to PdNPs and also the fastest hydrodechlorination: After the first substitution occurs, the second dechlorination can come along rapidly because the MCP molecule remains adsorbed due to the second activated Cl•••Pd bond and without release of the MCP.

4. Conclusion

In the H_2-based MPfR, the hollow-fiber membranes delivered H_2 and were the supporting material for PdNPs that formed to a stable film *in situ* and provided good reductive dechlorination of 2,4-DCP to P. The Pd-film was an efficient adsorbent for 2,4-DCP, and this was essential catalytic contact with activated H·. Operated in the continuous-flow mode, the MPfR gave nearly 90% reduction of 2,4-DCP to P. Kinetic modeling simulated well the HDC of 2,4-DCP in continuous-flow conditions and showed that the dominant pathway was full dechlorination of 2,4-DCP to P in adsorbed state. Small fractions were stepwise dechlorinated through 2-CP and 4-CP, which were released to the solution. DFT analysis suggests that the dominant pathway resulted from a thermodynamically favorable adsorption configuration. In summary, the experimental results and modeling indicate that full dechlorination of 2,4-DCP occurred primarily in the adsorbed state and with minimal release of MCPs, a desirable outcome for potential application of the MPfR technology.

Supporting Information

Experimental details, additional results of adsorption and HDC experiments, calculation process, and the results of DFT analysis were presented.

Declaration of Competing interest

The authors declare no competing financial interest.

Acknowledgements

This work is supported by National Natural Science Foundation of China (Grant No. NSFC 51678422) and the Fundamental Research Funds for the Central Universities.

Supplementary materials

Supplementary material associated with this article can be found, in the online version, at doi:10.1016/j.watres.2020.116465.

References

Benitez, J.L., Del Angel, G., 2000. Effect of chlorine released during hydrodechlorination of chlorobenzene over Pd, Pt and Rh supported catalysts. Reaction Kinetics and Catalysis Letters 70 (1), 67–72.
Besson, C., Finney, E.E., Finke, R.G., 2005. A Mechanism for Transition-Metal Nanoparticle Self-Assembly. J. Am. Chem. Soc. 127 (22), 8179–8184.
Buchel, K.H., 1984. Political, economic, and philosophical aspects of pesticide use for human welfare. Regulatory toxicology and pharmacology 4 (2), 174–191.
Chaplin, B.P., Reinhard, M., Schneider, W.F., Schueth, C., Shapley, J.R., Strathmann, T.J., Werth, C.J., 2012. Critical Review of Pd-Based Catalytic Treatment of Priority Contaminants in Water. Environ. Sci. Technol. 46 (7), 3655–3670.
Cho, Y.G., Rhee, S.K., Lee, S.T., 2000. Effect of soil moisture on bioremediation of chlorophenol-contaminated soil. Biotechnol. Lett. 22 (11), 915–919.
Conrad, H., Ertl, G., Latta, E.E., 1974. Adsorption of hydrogen on palladium single crystal surfaces. Surf Sci 41 (2), 435–446.
Deng, H., Fan, G., Wang, Y., 2014. Effective Hydrodechlorination of 4-Chlorophenol Over Pd Deposited on Multiwall Carbon Nanotubes. Synthesis and Reactivity in Inorganic Metal-Organic and Nano-Metal Chemistry 44 (9), 1306–1311.
Diaz, E., Mohedano, A.F., Casas, J.A., Rodriguez, J.J., 2016. Analysis of the deactivation of Pd, Pt and Rh on activated carbon catalysts in the hydrodechlorination of the MCPA herbicide. Applied Catalysis B-Environmental 181, 429–435.
Dolfing, J., Harrison, B.K., 1992. Gibbs free-energy of formation of halogenated aromatic-compounds and their potential role as electron-acceptors in anaerobic environments. Environ. Sci. Technol. 26 (11), 2213–2218.
Estevinho, B.N., Martins, I., Ratola, N., Alves, A., Santos, L., 2007. Removal of 2,4-dichlorophenol and pentachlorophenol from waters by sorption using coal fly ash from a Portuguese thermal power plant. J. Hazard. Mater. 143 (1–2), 535–540.
Fu, W., Shu, S., Li, J., Shi, X., Lv, X., Huang, Y.-X., Dong, F., Jiang, G., 2019. Identifying the rate-determining step of the electrocatalytic hydrodechlorination reaction on palladium nanoparticles. Nanoscale 11 (34), 15892–15899.
Gao, J., Liu, L., Liu, X., Zhou, H., Huang, S., Wang, Z., 2008. Levels and spatial distribution of chlorophenols 2,4-dichlorophenol, 2,4,6-trichlorophenol, and pentachlorophenol in surface water of China. Chemosphere 71 (6), 1181–1187.

Gao, Y., Sun, W., Yang, W., Li, Q., 2017. Creation of Pd/Al_2O_3 Catalyst by a Spray Process for Fixed Bed Reactors and Its Effective Removal of Aqueous Bromate. Sci Rep 7, 41797.
Jiang, G., Wang, K., Li, J., Fu, W., Zhang, Z., Johnson, G., Lv, X., Zhang, Y., Zhang, S., Dong, F., 2018. Electrocatalytic hydrodechlorination of 2,4-dichlorophenol over palladium nanoparticles and its pH-mediated tug-of-war with hydrogen evolution. Chemical Engineering Journal 348, 26–34.
Juhler, R.K., Sorensen, S.R., Larsen, L., 2001. Analysing transformation products of herbicide residues in environmental samples. Water Res. 35 (6), 1371–1378.
Khan, M., Khan, M., Kuniyil, M., Adil, S.F., Al-Warthan, A., Alkhathlan, H.Z., Tremel, W., Tahir, M.N., Siddiqui, M.R.H., 2014. Biogenic synthesis of palladium nanoparticles using Pulicaria glutinosa extract and their catalytic activity towards the Suzuki coupling reaction. Dalton Transactions 43 (24), 9026.
Kim, M.S., Chung, S.H., Yoo, C.J., Lee, M.S., Cho, I.-.H., Lee, D.W., Lee, K.Y., 2013. Catalytic reduction of nitrate in water over $Pd-Cu/TiO_2$ catalyst: effect of the strong metal-support interaction (SMSI) on the catalytic activity. Applied Catalysis B-Environmental 142, 354–361.
Langmuir, I., 1918. The adsorption of gases on plane surfaces of glass, mica and platinum. J. Am. Chem. Soc. 40 (9), 1361–1403.
Li, C., 2007. Voltammetric determination of 2-chlorophenol using a glassy carbon electrode coated with multi-wall carbon nanotube-dicetyl phosphate film. Microchimica Acta 157 (1–2), 21–26.
Shin, E.J., Keane, M.A., 1999. Detoxification of dichlorophenols by catalytic hydrodechlorination using a nickel/silica catalyst. Chem Eng Sci 54 (8), 1109–1120.
Shin, E.J., Spiller, A., Tavoularis, G., Keane, M.A., 1999. Chlorine-nickel interactions in gas phase catalytic hydrodechlorination: catalyst deactivation and the nature of reactive hydrogen. Physical Chemistry Chemical Physics 1 (13), 3173–3181.
Soares, O.S.G.P., Orfao, J.J.M., Pereira, M.F.R., 2009. Bimetallic catalysts supported on activated carbon for the nitrate reduction in water: optimization of catalysts composition. Applied Catalysis B-Environmental 91 (1–2), 441–448.
Sun, Z., Shen, H., Wei, X., Hu, X., 2014. Electrocatalytic hydrogenolysis of chlorophenols in aqueous solution on Pd58Ni42 cathode modified with PPy and SDBS. Chemical Engineering Journal 241, 433–442.
Tang, Y., Zhou, C., Van Ginkel, S.W., Ontiveros-Valencia, A., Shin, J., Rittmann, B.E., 2012. Hydrogen permeability of the hollow fibers used in H_2-based membrane biofilm reactors. J Memb Sci 407, 176–183.
United States Environmental Protection Agency, 2012. Drinking Water Standards and Health Advisories. Office of Water, U.S. EPA, Washington, D.C. EPA 822-B-00-001.
Vallecillo, A., Garcia-Encina, P.A., Pena, M., 1999. Anaerobic biodegradability and toxicity of chlorophenols. Water Science and Technology 40 (8), 161–168.
Wang, X., Yang, J., Zhu, M., Li, F., 2013. Characterization and regeneration of Pd/Fe nanoparticles immobilized in modified PVDF membrane. Journal of the Taiwan Institute of Chemical Engineers 44 (3), 386–392.
Wei, J., Xu, X., Liu, Y., Wang, D., 2006. Catalytic hydrodechlorination of 2,4-dichlorophenol over nanoscale Pd/Fe: reaction pathway and some experimental parameters. Water Res. 40 (2), 348–354.
Witthuhn, B., Klauth, P., Klumpp, E., Narres, H.D., Martinius, H., 2005a. Sorption and biodegradation of 2,4-dichlorophenol in the presence of organoclays. Appl Clay Sci 28 (1–4), 55–66.
Witthuhn, B., Pernyeszi, T., Klauth, P., Vereecken, H., Klumpp, E., 2005b. Sorption study of 2.4-dichlorophenol on organoclays constructed for soil bioremediation. Colloids and Surfaces a-Physicochemical and Engineering Aspects 265 (1–3), 81–87.
Xu, J., Cao, Z., Liu, X., Zhao, H., Xiao, X., Wu, J., Xu, X., Zhou, J.L., 2016a. Preparation of functionalized $Pd/Fe-Fe_3O_4$@MWCNTs nanomaterials for aqueous 2,4-dichlorophenol removal: interactions, influence factors, and kinetics. J. Hazard. Mater. 317, 656–666.
Xu, J., Liu, X., Lowry, G.V., Cao, Z., Zhao, H., Zhou, J.L., Xu, X., 2016b. Dechlorination Mechanism of 2,4-Dichlorophenol by Magnetic MWCNTs Supported Pd/Fe Nanohybrids: rapid Adsorption, Gradual Dechlorination, and Desorption of Phenol. ACS Appl Mater Interfaces 8 (11), 7333–7342.
Xu, J., Lv, X., Li, J., Li, Y., Shen, L., Zhou, H., Xu, X., 2012. Simultaneous adsorption and dechlorination of 2,4-dichlorophenol by Pd/Fe nanoparticles with multi-walled carbon nanotube support. J. Hazard. Mater. 225, 36–45.
Xu, J., Tan, L., Baig, S.A., Wu, D., Lv, X., Xu, X., 2013. Dechlorination of 2,4-dichlorophenol by nanoscale magnetic Pd/Fe particles: effects of pH, temperature, common dissolved ions and humic acid. Chemical Engineering Journal 231, 26–35.
Yuan, G., Keane, M.A., 2003a. Catalyst deactivation during the liquid phase hydrodechlorination of 2,4-dichlorophenol over supported Pd: influence of the support. Catal Today 88 (1–2), 27–36.
Yuan, G., Keane, M.A., 2003b. Liquid phase catalytic hydrodechlorination of 2,4-dichlorophenol over carbon supported palladium: an evaluation of transport limitations. Chem Eng Sci 58 (2), 257–267.
Yue, Q.Y., Yang, J., Gao, B.Y., Li, R.B., Li, Y., Yu, H., 2008. Adsorption characteristics of phenol compounds in water by activated carbon fiber. Huan jing ke xue 29 (10), 2862–2867.
Yuzhuo Chen, X.K., Mao, Shanjun, Wang, Zhe, Gong, Yutong, Wang, Yong, 2019. Study of the role of alkaline sodium additive in selective hydrogenation of phenol. Chinese Journal of Catalysis 40 (10), 1516–1524.
Zhang, J.F., Liu, H., Sun, Y.Y., Wang, X.R., Wu, J.C., Xue, Y.Q., 2005. Responses of the antioxidant defenses of the Goldfish Carassius auratus, exposed to 2,4-dichlorophenol. Environ. Toxicol. Pharmacol. 19 (1), 185–190.
Zhao, S., Zhao, C., Li, X., Li, F., Jiao, L., Gao, W., Li, R., 2016. Pd nanoparticles supported on amino-functionalized magnetic mesoporous silica nanotubes: a highly selective catalyst for the catalytic hydrodechlorination reaction. RSC Adv 6 (80), 76582–76589.
Zhou, C., Wang, Z., Marcus, A., Rittmann, B.E., 2016. Biofilm-Enhanced Continuous Synthesis and Stabilization of Palladium Nanoparticles (PdNPs). Environmental Science Nano 10, 1039 C1036EN00308G.
Zhou, C., Wang, Z., Ontiveros-Valencia, A., Long, M., Lai, C.Y., Zhao, H.P., Xia, S., Rittmann, B.E., 2017. Coupling of Pd nanoparticles and denitrifying biofilm promotes H_2-based nitrate removal with greater selectivity towards N_2. Applied Catalysis B Environmental 206, 461–470.